Journal of Materials Chemistry B

ROYAL SOCIETY OF CHEMISTRY

PAPER

View Article Online
View Journal | View Issue

Check for updates

Cite this: J. Mater. Chem. B, 2024, 12, 7618

A highly fluorescent and readily accessible all-organic photosensitizer model for advancing image-guided cancer PDT†

Andres Garcia-Sampedro, [a] Alejandro Prieto-Castañeda, [bc] Antonia R. Agarrabeitia, [bd] Jorge Bañuelos, [c] Inmaculada García-Moreno, [e] Angeles Villanueva, [fg] Santiago de la Moya, *[b] María J. Ortiz *[b] and Pilar Acedo *[a]

Received 23rd February 2024,
Accepted 1st July 2024

DOI: 10.1039/d4tb00385c

rsc.li/materials-b

The potential of using image-guided photodynamic therapy (ig-PDT) for cancer, especially with highly biocompatible fluorescent agents free of heavy atoms, is well recognized. This is due to key advantages related to minimizing adverse side effects associated with standard cancer chemotherapy. However, this theragnostic approach is strongly limited by the lack of synthetically-accessible and easily-modulable chemical scaffolds, enabling the rapid design and construction of advanced agents for clinical ig-PDT. In fact, there are still very few ig-PDT agents clinically approved. Herein we report a readily accessible, easy-tunable and highly fluorescent all-organic small photosensitizer, as a model design for accelerating the development and translation of advanced ig-PDT agents for cancer. This scaffold is based on BODIPY, which assures high fluorescence, accessibility, and ease of performance adaptation by workable chemistry. The optimal PDT performance of this BODIPY dye, tested in highly resistant pancreatic cancer cells, despite its high fluorescent behavior, maintained even after fixation and cancer cell death, is based on its selective accumulation in mitochondria. This induces apoptosis upon illumination, as evidenced by proteomic studies and flow cytometry. All these characteristics make the reported BODIPY-based fluorescent photosensitizer a valuable model for the rapid development of ig-PDT agents for clinical use.

Introduction

Theragnosis is a medical strategy consisting of performing therapy aided by *in situ* diagnosis using a single agent, being accounted as one of the most promising modern approaches for cancer treatment.[1,2] The simplest, most attractive and hopeful theragnostic agent is that based on a small organic photosensitizer (PS) able to generate both cytotoxic reactive oxygen species (ROS) and fluorescence upon specific illumination, enabling fluorescence-based image-guided PDT (ig-PDT).[3] Small size and organic nature are key for assuring proper absorption, distribution, metabolism and excretion, and therefore, minimal adverse effects in absence of illumination (low dark toxicity).[4]

However, designing small-sized fluorescent molecules for ig-PDT is challenging, since the required photonic behaviours (ROS photogeneration and fluorescence) are antagonistic when coming from the same fluorophore (the higher the fluorescence efficiency, the lower the ROS production). Therefore, these characteristics must be precisely counterbalanced to reach the desired theragnostic efficiency.[5,6] In this context, potentially toxic heavy atoms are usually involved in the ig-PDT structure, as the main approach to increase ROS production and enhance PDT efficiency. However, this is detrimental for fluorescence-based diagnosis and to ensure low dark toxicity.[7]

We and others have recently demonstrated that highly fluorescent PSs can enable efficient PDT when they accumulate in PDT-sensitive cell organelles, such as lipid droplets[8] or

[a] Institute for Liver and Digestive Health, Royal Free Hospital Campus, University College London, Pond Street, London NW3 2QG, UK. E-mail: p.nunez@ucl.ac.uk
[b] Departamento de Química Orgánica, Facultad de Ciencias Químicas, Universidad Complutense de Madrid, Ciudad Universitaria s/n, 28040 Madrid, Spain. E-mail: santmoya@ucm.es, mjortiz@quim.ucm.es
[c] Departamento de Química-Física, Universidad del País Vasco-EHU, 48080 Bilbao, Spain
[d] Sección Departamental de Química Orgánica, Facultad de Óptica y Optometría, Universidad Complutense de Madrid, Arcos de Jalón 118, 28037 Madrid, Spain
[e] Departamento de Química-Física de Materiales, Instituto de Química-Física Blas Cabrera, Consejo Superior de Investigaciones Científicas (CSIC), Serrano 119, 28006 Madrid, Spain
[f] Departamento de Biología, Universidad Autónoma de Madrid, Darwin 2, 28049 Madrid, Spain
[g] Instituto Madrileño de Estudios Avanzados (IMDEA) Nanociencia, Ciudad Universitaria de Cantoblanco, 28049 Madrid, Spain

† Electronic supplementary information (ESI) available. See DOI: https://doi.org/10.1039/d4tb00385c

mitochondria.[9] This fact paves the way for advancing cancer ig-PDT avoiding toxic heavy atoms to gain PDT action. Moreover, a high fluorescence for efficient imaging can also be achieved.

Mitochondria accumulation is particularly interesting for ig-PDT. This is due to the importance of mitochondria health for cell survival and to chemical ease for promoting the accumulation of organic compounds within mitochondria. Regarding the first fact, healthy mitochondria are fundamental for cell survival as these organelles are involved in multiple key processes, including cell metabolism, stress response or calcium homeostasis.[10] Moreover, in connection with cancer PDT, mitochondria is pivotal in maintaining ROS balance within cells,[11] as well as in cancer signalling pathways.[12] Indeed, there is a growing interest in the development of mitochondria-targeting PDT agents.[13]

Related to the second fact, the negative mitochondrial membrane potential, hyperpolarised mitochondrial transmembrane voltage (Ψ_{IM}) *ca.* −140 mV in normal cells and *ca.* −220 mV in cancer cells, promotes the accumulation of organic cationic species possessing high capability to permeate lipophilic membranes.[14] These species can be easily achieved by involving delocalized cations (*e.g.*, common triphenylphosphonium cation) in lipophilic-enough organic scaffolds, to construct the so-called membrane-permeable delocalized lipophilic cations (DLCs).[15–17]

The known high lipophilicity of BODIPY (boron dipyrromethene) dyes, joint to their easy synthesis and tuneability by workable organic chemistry, make them first-choice scaffolds for the development of advanced ig-PDT agents based on fluorescent and membrane-permeable DLCs. In fact, mitochondria-targeting BODIPY-based DLCs have been recently developed as fluorescent mitochondria probes for bioimaging purposes,[17–22] as well as agents for several image-guided photo-triggered therapies.[23,24] However, the BODIPY-based DLC approach has been scarcely explored to develop fluorescent PSs for ROS-based ig-PDT, and the up-to-now reported few PDT PSs based on this approach are poorly fluorescent or involve heavy atoms.[25–27]

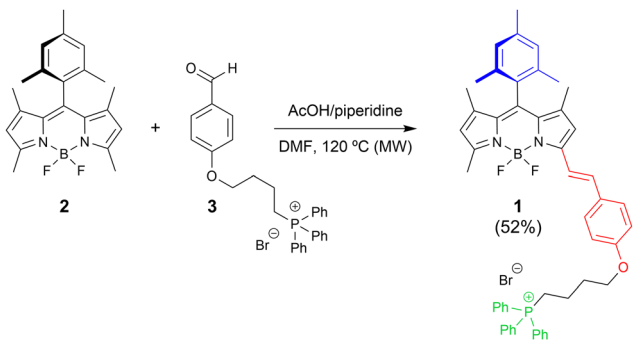

Fig. 1 Synthesis of BODIPY **1** as a fluorescent scaffold for cancer ig-PDT. Design structural keys: *meso*-mesityl for bright fluorescence (in blue); π-conjugated electron-rich alkoxystyryl for red-shifting (in red); and triphenylphosphonium for mitochondria accumulation (in green). See ESI† for experimental details. DMF = *N*,*N*-dimethylformamide. MW = microwaving. AcOH = acetic acid.

This scenario prompted us to develop an accessible and highly fluorescent PDT PS based on both BODIPY and mitochondrial accumulation (see **1** in Fig. 1).[9] Such an agent could serve as a valuable model scaffold for the development of sought-after clinical ig-PDT agents for cancer treatment.[3,28] As a proof of concept, we have applied and tested the performance of BODIPY **1** as a fluorescent mitochondria-targeting ig-PDT agent in highly aggressive and resistant pancreatic cancer cells used as a disease model. Normal human pancreatic duct epithelial (H6c7) cells were employed to evaluate BODIPY **1** dark toxicity.

Results and discussion

Molecular design and synthesis

We designed heavy-atom free BODIPY **1** (Fig. 1) taking into account the following premises: (1) structural simplicity; (2) rapidly constructing a highly fluorescent red-shifted BODIPY dye (note the relevance of red-shifting the agent's light absorption region for clinical PDT[29,30]); and (3) rapidly constructing a BODIPY-based DLC.

Thus, BODIPY **1** should be easily synthesized from available starting materials by means of the well-known Knoevenagel BODIPY post-functionalization approach, which is commonly used to construct red-shifted styrylated BODIPYs from precursors involving acidic-enough methyl groups.[29] Moreover, the presence of mesityl at the BODIPY *meso* position was selected to enhance dye lipophilicity without losing fluorescence efficiency (note methyl–methyl clash avoiding fluorescence quenching by mesityl rotation).[31]

Satisfactorily, BODIPY **1** was obtained straightforwardly (52% yield) by Knoevenagel-like condensation of accessible 8-mesityl-1,3,5,7-tetramethyl-F-BODIPY **2**[32] with triphenylphosphonium-based benzaldehyde **3**[33] under standard conditions (acetic acid/piperidine activation; see Fig. 1).

Photophysical characterization

Expectedly, the involvement of the functionalized styryl moiety led to a π-extended BODIPY chromophoric core, pushing its main spectral bands to the red edge of the visible spectrum (Fig. S1 in ESI†). As consequence, BODIPY **1** displayed a sharp and intense absorption at 571 nm (molar absorption up to 45 000 M^{-1} cm^{-1}) in chloroform solution, followed by a strong fluorescence emission (fluorescence quantum yield, ϕ, equal to 80%) at 580 nm, thus approaching the spectral biological window (see Fig. S1, ESI†). In spite of its brilliant emission, the new probe was also able to render a dim emission at 1280 nm, owing to singlet oxygen phosphorescence. This phosphorescent signal allowed us to quantify a singlet-oxygen photogeneration quantum yield, ϕ_Δ, equal to 4% (see ESI† for details). All these photophysical results in organic solvent solution anticipated that BODIPY **1** should enable a glow fluorescent bioimaging, but a limited singlet oxygen photogeneration (PDT Type II mechanism), albeit PDT could be viable by the photo-generation of other ROS in biological media

(PDT Type I mechanism).[30,34,35] The natural transition orbitals (NTO) analysis for the S_1 state (see ESI† for computational details) revealed that, although there is a significant hole–electron overlap with S_0, the charge density had been shifted from the alkoxystyryl moiety to the BODIPY core (see Fig. S1 in ESI†). Accordingly, the involved excited state would possess a dual hybridized local and charge transfer (HLCT) character.[36,37] It must be noted that HLCT states are particularly suited for ig-PDT because they are emissive enough, and can additionally serve as gateways to populate energetically-close triplet states for $^1O_2$ generation (Type II PDT mechanism). Besides, the weakly bounded charge-separated HLCT excitons are prone to undergo oxidation/reduction processes, paving the way for the generation of ROS by the Type I mechanism. Indeed, conducted cyclic voltammetry (see ESI† for experimental details) anticipates that BODIPY **1** is susceptible to be reduced at the strongly bounded ground state (at −0.83 V; see Fig. S1 in ESI†), supporting its capability to be efficiently reduced by biological reductants in its excited state. Noteworthy, although the involved polar phosphonium cation is not enough to overcome the common low solubility of standard BODIPYs in water, it endows probe **1** with enough hydrophilicity to be fully soluble in aqueous culture media at standard probe-working concentrations, as well as to display a relatively high fluorescence efficiency in water (ϕ = 31%).

Additionally, another photonic key property for gaining photo-theragnostic efficiency is the dye photostability under severe, long-term laser pumping conditions, mimicking those involved in high-resolution microscopy techniques. Interestingly, BODIPY **1** unveils as a highly photostable dye since it was

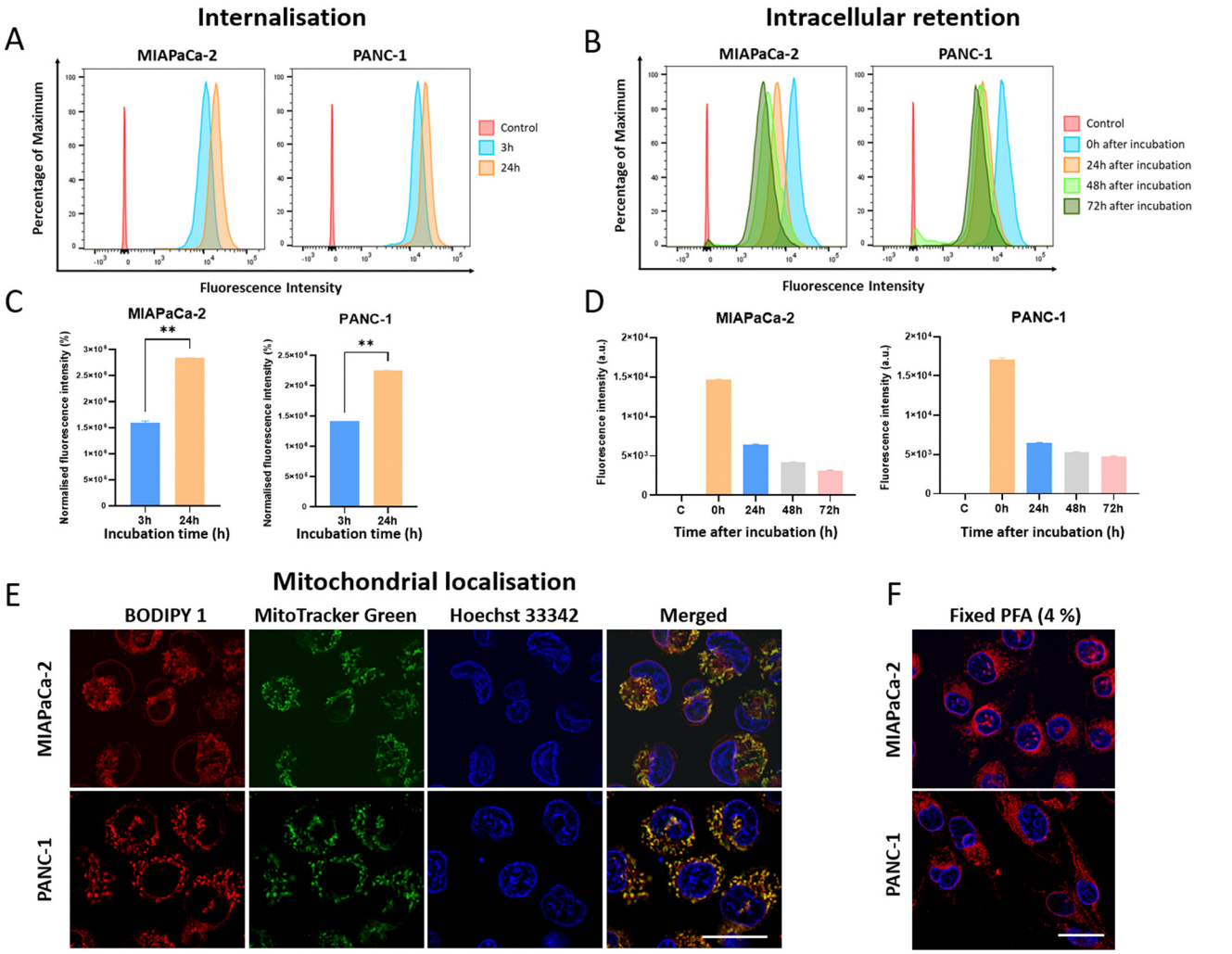

Fig. 2 Cellular internalization and subcellular localization of BODIPY **1** in pancreatic cancer cells. (A) Flow cytometry histograms showing the uptake of BODIPY **1** (1 μM) in MIAPaCa-2- and PANC-1 cells at 3 h (blue histogram) or 24 h incubation (orange histogram). Untreated control cells are shown in red. (B) Time of retention of the probe inside the cells. Cells were incubated with 1 μM BODIPY **1** for 3 h, thoroughly washed and fluorescence was analysed using flow cytometry at 0 h (blue), 24 h (orange), 48 h (light green) or 72 h (dark green) post-incubation. Background fluorescence of untreated cells is shown in red for comparison. (**C**) and (D) Quantification of the median fluorescence intensity shown in A and B. $^{**}p < 0.01$. (E) Live-cell microscopy showing subcellular localization of BODIPY **1** (500 nM) after incubation for 30 min. Mitochondria were counterstained in green with MitoTracker™ Green, and nuclei with Hoechst 33342. Scale bar = 25 μm. (F) PANC-1 and MIAPaCa-2 cells incubated with 500 nM BODIPY **1** for 30 min and fixed with 4% PFA showing BODIPY **1** fluorescence in red. Nuclei were counterstained in blue. Scale bar = 20 μm. See ESI† for details.

able to sustain its initial laser-induced fluorescent emission without degradation signs after 50 000 laser pulses (see ESI† for details).

ig-PDT performance

The photo-theragnostic potential of BODIPY **1** was tested in two human pancreatic cancer cell lines: MIAPaCa-2 and, which is more relevant, the chemo-resistant PANC-1 cells.[38,39] Moreover, for IC50 value calculations and evaluation of BODIPY **1** dark toxicity and localization, normal human pancreatic duct epithelial (H6c7) cells were used.

BODIPY **1** was internalized by both pancreatic cancer cell lines in a quick fashion, as shown by flow cytometry analysis (see Fig. 2A and C). This fact demonstrated the expected high capability of BODIPY **1** to permeate cell membranes on the basis of its lipophilic character and small size. In terms of intracellular retention, the concentration of the dye inside the cells was reduced by 56.24–62.05% in the first 24 h after incubation in MIAPaCa-2 and PANC-1 cells, respectively, which was further reduced by 78.43–72.14% after 72 h. This highlights its rapid clearance once the cells are no longer in contact with the dye, which could minimise toxicity (see Fig. 2B and D).

In addition, BODIPY **1** resulted as a very good and stable fluorescent mitochondrial probe (already at a nanomolar concentration), as expected by its DLC character and confirmed by co-localization experiments performed with MitoTracker™ Green (see Fig. 2E and Fig. S2C, ESI†). BODIPY **1** and the commercial mitochondrial probe showed a Pearson's correlation coefficient (PCC) of 0.77 and 0.91 in MIAPaCa-2 and PANC-1 cultures, respectively. Thus, BODIPY **1** was able to quickly accumulate in the mitochondria of live pancreatic cancer cells (30 min incubation with 500 nM of dye), displaying high photostability and intense fluorescence emission upon light excitation. Furthermore, its specific mitochondrial localization was maintained after live-cell labelling fixation with 4% paraformaldehyde (PFA) (see Fig. 2F).

Next, the photobiological activity of BODIPY **1** was analysed in-depth in both human pancreatic ductal adenocarcinoma (PDAC) cell lines. The PDT effect was extremely lethal (see Fig. 3). Both cell lines have epithelial-to-mesenchymal transition differentiation but since PANC-1 cells do not express E-cadherin, its behaviour is more aggressive with a greater metastasizing potential.[38,39] These results confirmed the developed BODIPY dye as optimal for the desired proof of concept, since it is highly bright and accumulates selectively into mitochondria due to its DLC character. To our satisfaction, and despite of its poor singlet-oxygen photosensitizing capability, the dye was able to act as an efficient PDT agent even under excitation below its maximum absorption (525 nm; IC_{50} = 501–640 nM; light dose = 10.3 J cm^{-2}), as demonstrated by metabolic activity assays (see Fig. 3A and B). Cell viability after PDT treatment with selected concentrations of BODIPY **1** was further validated by flow

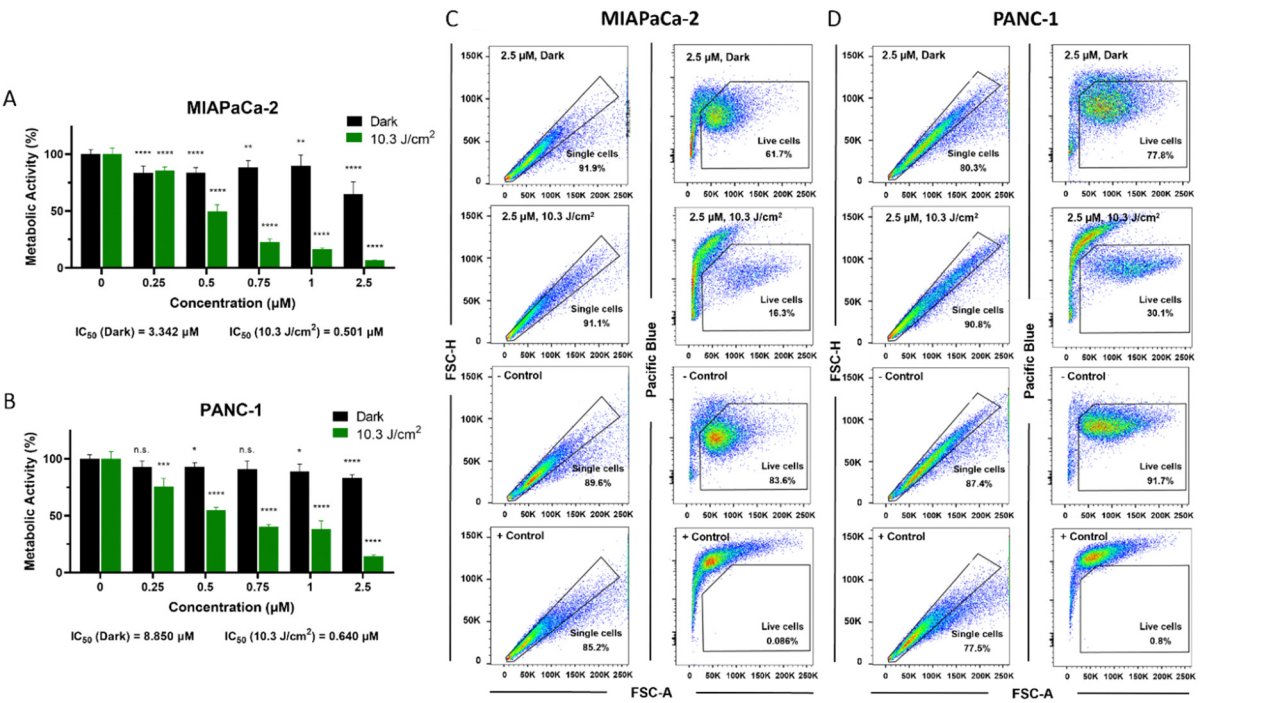

Fig. 3 Photodynamic therapy (PDT) performance for pancreatic cancer cells using BODIPY **1** as photosensitizer. (A) and (B) Percentage of total metabolic activity after PDT treatments with BODIPY **1** in MIAPaCa-2 (A) or PANC-1 cells (B) incubated with the probe for 3 h. Green bars show metabolic activity 48 h after illumination (10.3 J cm^{-2} light dose), and black bars represent toxicity in dark conditions (non-illuminated group). Statistically significant differences are labelled as n.s. not significant, *$p < 0.05$, **$p < 0.01$, ***$p < 0.001$, ****$p < 0.0001$ for comparisons with untreated groups (0 μM). (C) and (D) Cell viability after BODIPY **1** PDT in MIAPaCa-2 (C) or PANC-1 cells (D) analysed by flow cytometry. Untreated cells (− control) and cells treated with 70% ethanol (+ control) are shown for comparison. Representative dot plots are shown per condition. A total number of at least 20 000 cells were analysed per group. See ESI† for details.

cytometry (Fig. 3C and D). It must be highlighted here that, despite some BODIPYs have been described as good mitochondrial fluorescent probes, they did not produce photo-cytotoxic effects, and therefore, would not have therapeutic potential to treat cancer.[17–22,40]

As expected, PANC-1 cells showed higher resistance to therapy than MIAPaCa-2 (30.1% *vs.* 18.3% live cells after 1 μM BODIPY **1** PDT). However, increasing BODIPY **1** concentration to 2.5 μM induced a lethal effect in both cell lines. Dark toxicity of the dye was also evaluated by MTT assays, flow cytometry and LIVE/DEAD staining, including in normal human pancreatic duct epithelial (H6c7) cells (see Fig. 3 and Fig. S2, ESI†), showing minimal effect on the cells at the tested concentrations (83.6–91.7% live cells), supporting its high biocompatibility, as designed for it (heavy-atom-free small-sized BODIPY dye). The calculations of the IC50 values for dark toxicity shown in Fig. S3 (ESI†) were based on cell incubation with BODIPY 1 at concentrations ranging from 0.25 μM to 25 μM.

Therefore, based on all these promising obtained data, we expect the photo-theranostic properties of BODIPY **1** could also be applied to other types of human solid tumors. Note BODIPY **1** is expected to be more effective as ig-PDT agent under optimized irradiation at its maximum absorption, resulting in greater PDT cytotoxicity and fluorescence.

Biomolecular mechanism of action

Once the potential of BODIPY **1** as ig-PDT agent was confirmed, we proceeded to investigate the biomolecular mechanism of the PDT action triggering cell death.

For this purpose, ROS production in cells after 10.3 J cm^{-2} PDT was measured by incubating samples with the fluorescent ROS probe H2DCFDA (see Fig. 4A and B). MIAPaCa-2 cells showed an increased ROS generation (91.97% average positive cells) compared to PANC-1 (13.36%) using the same BODIPY **1** dose (1 μM, 3 h incubation time). This was in line with previous photo-toxicity results indicating an increased sensitivity of MIAPaCa-2 cells to PDT.[41]

However, when a higher dose of the dye was used (2.5 μM), both cell lines showed increased ROS levels (89.19% and 64.14%, respectively; see Fig. 4A and B), suggesting that the

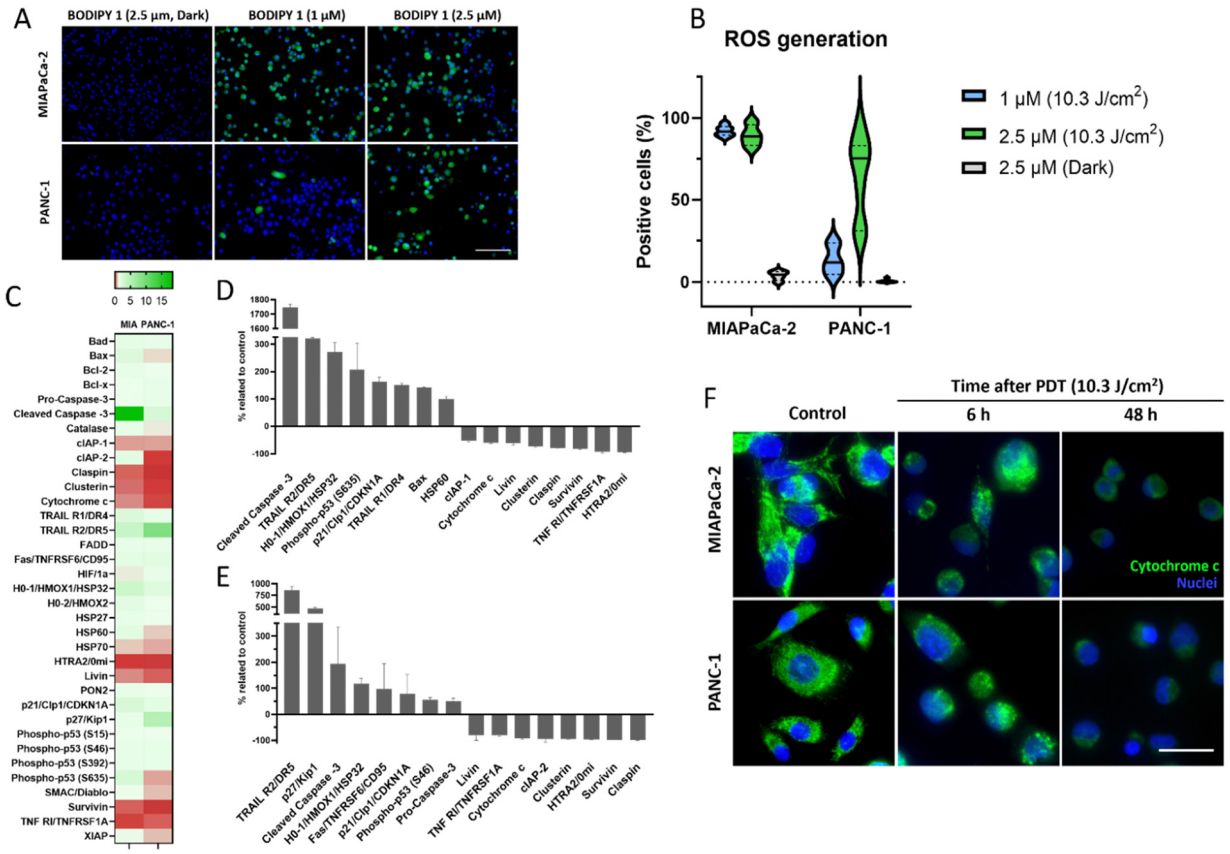

Fig. 4 Molecular mechanism of action of BODIPY **1** as photosensitizer for PDT. (A) Generation of reactive oxygen species (ROS) in pancreatic cancer cells after 3 h incubation with BODIPY **1** followed by illumination (10.3 J cm^{-2} light dose). Cells were preincubated with the ROS probe H2DCFDA, displaying green fluorescence. Nuclei were counterstained in blue. Scale bar = 100 μm. (B) Violin plots with the quantification of ROS-positive cells after illumination. (C) Heatmap of the proteomic analysis of a panel of 35 proteins directly involved in cell death mechanisms. Squares represent overexpression (green) or underexpression (red) of proteins in MIAPaCa-2 (MIA) or PANC-1 cells treated with BODIPY **1** compared to untreated controls. (D) and (E) Boxplot comparison of the top five most upregulated and downregulated proteins observed in MIAPaCa-2 (D) and PANC-1 (E) cells after treatment. (F) Immunofluorescence of cytochrome *c* (green) in cells treated with BODIPY 1 (2.5 μM) at 6 h and 48 h after treatment. Scale bar = 50 μm.

resistance to therapy of PANC-1 cells can be overcome with a minimal increase in the BODIPY dose. These high levels of in-cell ROS are not in disagreement with the shown poor ability of BODIPY **1** to act as a singlet oxygen photo-generator (see photophysical characterization section above), and demonstrate that cytotoxic ROS generation can be boosted in cells, inducing cytotoxicity when small ROS amounts are located in specific, key cell targets, such as mitochondria. In addition, the said highly biocompatible nature of this dye was supported by the minimal ROS production in the absence of light irradiation (dark conditions; 3.88% and 0.52%, respectively; see Fig. 4A and B). Overall, these results confirm that BODIPY **1** can enhance ROS generation upon light activation in the subcellular microenvironment of pancreatic cancer cells, potentially altering the redox balance and triggering cell death.

In order to elucidate the molecular cascade triggered by photo-damage and ROS production, as well as the cell death subtype induced after BODIPY **1** PDT, we performed a proteomic analysis of 35 proteins directly involved in cell death mechanisms in MIAPaCa-2 and PANC-1 cells treated with 2.5 μM BODIPY **1** and a light dose of 10.3 J cm^{-2} (Fig. 4C–E).

Remarkably, at 48 h after PDT treatment, both pancreatic cancer cell lines showed a drastic increase in the intracellular levels of cleaved (active) caspase-3 compared to untreated controls (see Fig. 4C–E). Caspase-3 has been identified as a key apoptosis mediator, activated in apoptotic cells by both extrinsic (death ligands) and intrinsic (mitochondrial) pathways. Active caspase-3 is reported to cleave structural proteins as well as cell cycle proteins and DNases, causing blebbing and condensation of the DNA, strong indicators of apoptosis induction.[42] Assessment of key apoptotic morphological changes induced after PDT were performed using neutral red staining (see Fig. S4 in ESI†), which confirmed these results.

Similarly, increased expression of death receptors TRAIL R2/DR5 and TRAIL R1/DR4 was observed (see Fig. 4C–E), which supports the hypothesis of apoptosis as the principal cell death mechanism induced by BODIPY **1** PDT. Previously reported *in vivo* studies have proven that increased expression of these receptors selectively triggers apoptotic death of cancer cells, sparing toxicity to non-malignant cells.[43,44] Moreover, other proteins involved in response to oxidative stress, such as Heme oxygenase-1 (HO-1/HMOX1/HSP32), were overexpressed after treatment (see Fig. 4C–E), confirming the protective response of pancreatic cancer cells to increased ROS levels generated after BODIPY **1** PDT. Two opposite regulatory roles of HO-1 in mitochondrial function have been described as mitigating or exacerbating oxidative stress, and these can depend on the overall cell ROS levels and cancer type.[45] HO-1 has been reported to have an anti-proliferative and pro-apoptotic activity[43]. Interestingly, some studies have attributed HO-1 a cytoprotective role, promoting angiogenesis and cancer cell survival.[45] Consequently, various HO-1 inhibitors are currently under investigation to enhance therapeutic response.[46] Overall, our results highlight the advantages of BODIPY **1** for PDT, as it promotes ROS generation, inducing apoptotic cell death by caspase 3 activation and upregulation of death receptors.

In contrast, the expression of claspin was reduced after BODIPY **1** PDT treatment in both cancer cell lines (see Fig. 4C–E). This highly preserved checkpoint adaptor and DNA replication factor has been shown to be cleaved by caspase-7 during apoptosis.[44] In pancreatic cancer, claspin has also been associated with tumour progression and resistance to therapy.[47]

Another key protein is survivin, an inhibitor of apoptosis that is found overexpressed in PDAC tumours.[48] In our models, survivin levels decreased after BODIPY **1** PDT (see Fig. 4C–E), suggesting once again the induction of the apoptotic pathway, and a possible strategy to avoid resistance to therapy. Likewise, two other inhibitors of apoptosis (cIAP-1 and cIAP-2) were downregulated after PDT (see Fig. 4C–E). Interestingly, a reduction in HTRA2/Omi (a pro-apoptotic mitochondrial serine protease involved in caspase-dependent cell apoptosis),[48] together with a minimally dysregulated expression of XIAP (X-linked inhibitor of apoptosis),[49] suggest that the apoptosis extrinsic pathway may be favoured as opposed to the intrinsic pathway. However, further protein expression studies involving key factors of that route should be performed to validate these findings.

Lastly, immunofluorescence staining of cytochrome *c* showed a mitochondrial localisation in untreated cells (pre-PDT), where cytochrome *c* plays its role in ATP synthesis (Fig. 4F). Upon light activation of BODIPY **1**, cytochrome *c* translocated from the mitochondria to the cytosol where it binds to SMAC and HTRA2, ultimately promoting apoptosis.[50] Delocalization of cytochrome *c* was already visible at 6 h post treatment, and it was increased at 48 h. Finally, we also evaluated rearrangements in the microtubule cytoskeleton induced post BODIPY **1** PDT by α-tubulin immunofluorescence, as the cytoskeleton plays a key role in the migratory and metastatic phenotype of tumor cells. As shown in ESI† Fig. S5, untreated MIAPaCa-2 and PANC-1 cells displayed normal distribution of tubulin in the cytoplasm. However, cells treated with BODIPY **1** + PDT (2.5 μM, 10.3 J cm^{-2}) showed a round apoptotic shape and a profound cytoskeleton disorganization, indicative of microtubule destabilization, with noticeable formation of retraction fibres and microtubule remodelling.

Conclusions

In summary, we have developed a structurally simple BODIPY dye serving as chromophoric model for the rapid construction of sought-after ig-PDT agents. These agents should pave the way for efficient cancer treatment with minimal adverse effects, as herein demonstrated against highly aggressive pancreatic cancer cells and in dark toxicity experiments performed in normal human pancreatic duct epithelial (H6c7) cells. Key characteristics of the developed BODIPY scaffold are: significant ig-PDT performance in spite of its simplicity and the absence of heavy atoms; easy synthesis from readily accessible materials; possibility of further optimizations by workable BODIPY chemistry (*e.g.*, aimed at increasing PDT efficiency, promoting actuation in the near-infrared (NIR) spectral region, or increasing selectivity by tumour recognition).

Regarding ig-PDT performance, on the one hand, the highly fluorescent BODIPY **1** behaves as an efficient and photostable fluorescent mitochondrial probe, rapidly internalizing into the cells and accumulating within mitochondria, as confirmed by flow cytometry analysis and co-localization experiments by confocal microscopy with MitoTracker™ Green, respectively. On the other hand, upon illumination, poorly cytotoxic BODIPY **1** also acts as an efficient heavy-atom free PDT PS in highly resistant pancreatic cancer cells, boosting ROS generation, caspase-3 activation and triggering apoptotic death, cytochrome *c* translocation and cytoskeleton disorganization, while decreasing the levels of survivin, claspin and cIAPs.

These results also remark the capability of mitochondria to serve as a very sensitive intracellular target for performing photo-theragnostic ig-PDT, even by using highly fluorescent heavy-atom free PDT agents, as well as the possibility of rapidly achieving ig-PDT agents by easily constructing highly fluorescent BODIPY-based DLCs.

The excellent behaviour of heavy-atom free BODIPY **1**, as a highly fluorescent PS boosting ROS production, mainly under the Type I mechanism, enabling efficient PDT action upon non-optimized illumination, joint to key advantages derived from BODIPY-dye nature, such as synthetic accessibility, easy adaptability by workable chemistry, and chemical and photophysical robustness, should encourage further investigations on its use as a valuable chromophoric scaffold for advancing the development of mitochondria-targeting agents to be approved for cancer ig-PDT treatment. Future studies will include *in vivo* validation. Combination treatment approaches could be explored involving BODIPY **1** and chemotherapy, or a dual treatment with HO-1 inhibitors to achieve a synergistic or adjuvant effect on treatment resistance.

Author contributions

The manuscript was written through contributions of all authors. All authors have given approval to the final version of the manuscript.

Data availability

The data supporting this article have been included as part of the ESI.†

Conflicts of interest

There are no conflicts to declare.

Acknowledgements

Authors acknowledge grants PID2020-114755GB-C31, -C32 and -C33 funded by Spanish MCIN/AEI/10.13039/501100011033, and grant IT1639-22 funded by Basque Government. A. P.-C. thanks grant FJC2021-046650-I funded by MCIN/AEI/10.13039/501100011033 and by the European Union NextGenerationEU/PRTR. P. A. thanks funding from Pancreatic Cancer UK and the Ramon Areces Foundation.

References

1 S. Jeyamogan, N. A. Khan and R. Siddiqui, *Arch. Med. Res.*, 2021, **52**, 131–142.
2 B. J. Burkett, D. J. Barlett, P. W. McGarrah, A. R. Lewis, D. R. Johnson, K. Berberoğlu, M. K. Pandey, A. T. Packard, T. R. Halfdanarson, C. B. Hruska, G. B. Johnson and A. T. Kendi, *Radiol. Imag. Cancer*, 2023, **5**, e220157.
3 P. Sarbadhikary, B. P. George and H. Abrahamse, *Theranostics*, 2021, **11**, 9054–9088.
4 J. Zhang, L. Ning, J. Huang, C. Zhang and K. Pu, *Chem. Sci.*, 2020, **11**, 618–630.
5 H. Kim, G. Kwak, K. Kim, H. Y. Yoon and I. C. Kwon, *Biomaterials*, 2019, **213**, 119207.
6 P. Cheng and K. Pu, *ACS Appl. Mater. Interfaces*, 2020, **12**, 5286–5299.
7 T. C. Pham, V.-N. Nguyen, Y. Choi, S. Lee and J. Yoon, *Chem. Rev.*, 2021, **121**, 13454–13619.
8 A. Tabero, F. García-Garrido, A. Prieto-Castañeda, E. Palao, A. R. Agarrabeitia, I. García-Moreno, A. Villanueva, S. de la Moya and M. J. Ortiz, *Chem. Commun.*, 2020, **56**, 940–943.
9 M. J. Ortiz, A. R. Agarrabeitia, S. de la Moya, T. Mazuelo-Santos, A. Prieto-Castañeda, A. Villanueva, A. Tabero, P. Acedo and A. García-Sampedro, *Nuevos colorantes BODIPY para teragnosis fotodinámica basados en acumulación en mitocondrias*, *ES Pat.*, ES2800548A1 (30.12.2020), ES2800548B2 (09.07.2021).
10 C. Giorgi, S. Marchi and P. Pinton, *Nat. Rev. Mol. Cell Biol.*, 2018, **19**, 713–730.
11 V. Brillo, L. Chieregato, L. Leanza, S. Muccioli and R. Costa, *Life*, 2021, **11**, 332.
12 P. Jin, J. Jiang, L. Zhou, Z. Huang, E. C. Nice, C. Huang and L. Fu, *J. Hem. Oncol.*, 2022, **15**, 97.
13 M. D. Yaqoob, L. Xu, C. Li, M. M. L. Leong and D. D. Xu, *Photodiagn. Photodyn. Ther.*, 2022, **38**, 102830.
14 J. S. Modica-Napolitano and J. R. Aprille, *Adv. Drug Delivery Rev.*, 2001, **49**, 63–70.
15 J. Zielonka, J. Joseph, A. Sikora, M. Hardy, O. Ouari, J. Vasquez-Vivar, G. Cheng, M. Lopez and B. Kalyanaraman, *Chem. Rev.*, 2017, **117**, 10043–10120.
16 J. Y. Wang, J. Q. Li, Y. M. Xiao, B. Fu and Z. H. Qin, *ChemMedChem*, 2020, **15**, 404–410.
17 H. Crawford, M. Dimitriadi, J. Bassin, M. T. Cook, T. F. Abelha and J. Calvo-Castro, *Chem. – Eur. J.*, 2022, **28**, e202202366.
18 X. Song, N. Li, C. Wang and Y. Xiao, *J. Mater. Chem. B*, 2017, **5**, 360–368.
19 T. Gao, H. He, R. Huang, M. Zheng, F.-F. Wang, Y.-J. Hu, F.-L. Jiang and Y. Liu, *Dyes Pigm.*, 2017, **141**, 530–535.
20 D. K. Mai, I. W. Badon, J. M. Lim, T. P. Vales, C. Kim, J. Yang, J. Lee and H.-J. Kim, *Dyes Pigm.*, 2022, **208**, 110856.

21 W.-J. Shi, Y.-F. Wei, J. Yang, H.-Z. Li, Q.-H. Wan, Y. Wang, H. Leng, K. Cheng and J.-W. Yan, *Sens. Actuators, B*, 2022, **359**, 131594.
22 J.-L. Wang, L. Zhang, L.-X. Gao, J.-L. Chen, T. Zhou, Y. Liu and F.-L. Jiang, *J. Mater. Chem. B*, 2021, **9**, 8639–8645.
23 R. Tiwari, P. S. Shinde, S. Sreedharan, A. K. Dey, K. A. Vallis, S. B. Mhaske, S. K. Pramanik and A. Das, *Chem. Sci.*, 2021, **12**, 2667–2673.
24 J.-L. Wang, L. Zhang, M.-J. Zhao, T. Zhang, Y. Liu and F.-L. Jiang, *ACS Appl. Bio Mater.*, 2021, **4**, 1760–1770.
25 T. P. Vales, S. Cho, J. Lee, H. T. Bui, D. K. Mai, I. W. Badon, H. Lim, W. Jeong, J.-L. Kim, H.-K. Kim and H.-J. Kim, *J. Mol. Struct.*, 2021, **1246**, 131284.
26 I. W. Badon, C. Kim, J. M. Lim, D. K. Mai, T. P. Vales, D. Kang, S. Cho, J. Lee, H.-J. Kim and J. Yang, *J. Mater. Chem. B*, 2022, **10**, 1196–1209.
27 W. I. Badon, J.-P. Jee, T. P. Vales, C. Kim, S. Lee, J. Yang, S. K. Yang and H.-J. Kim, *Pharmaceutics*, 2023, **15**, 1512.
28 H.-B. Cheng, X. Cao, S. Zhang, K. Zhang, Y. Cheng, J. Wuang, J. Zhao, L. Zhou, X.-J. Liang and J. Yoon, *Adv. Mater.*, 2023, **35**, 2207546.
29 H. Lu, J. Mack, Y. Yang and Z. Shen, *Chem. Soc. Rev.*, 2014, **43**, 4778–4823.
30 Z. Mao, J. H. Kim, J. Lee, H. Xiong, F. Zhang and J. S. Kim, *Coord. Chem. Rev.*, 2023, **476**, 214908.
31 S. V. Mulay, T. Yudhistira, M. Choi, Y. Kim, J. Kim, Y. J. Jang, S. Jon and D. J. Churchill, *Chem. – Asian J.*, 2016, **11**, 3598–3605.
32 L. Fu, F.-L. Jiang, D. Fortin, P. D. Harvey and Y. Liu, *Chem. Commun.*, 2011, **47**, 5503–5505.
33 S. Patil, S. Pandey, A. Singh, M. Radhakrishna and S. Basu, *Chem. – Eur. J.*, 2019, **25**, 8229–8235.
34 Z. Zhou, J. Song, L. Nie and X. Chen, *Chem. Soc. Rev.*, 2016, **45**, 6597–6626.
35 D. van Straten, V. Mashayekhi, H. S. de Bruijn, S. Oliveira and D. J. Robinson, *Cancers*, 2017, **9**, 19.
36 C. Li, Y. Guo, M. Zhao, Y. Pan and B. Yang, *Comput. Theor. Chem.*, 2021, **1200**, 113247.
37 X. Nie, Z. Mahmood, D. Liu, M. Li, D. Hu, W. Chen, L. Xing, S. Su, Y. Shuo and S. Ji, *Energy Environ. Mater*, 2024, **7**, e12597.
38 R. Gradiz, H. C. Silva, L. Carvalho, M. F. Botelho and A. Mota-Pinto, *Sci. Rep.*, 2016, **6**, 21648.
39 Y. Shen, K. Pu, K. Zheng, X. Ma, J. Qin, L. Jiang and J. Li, *Int. J. Mol. Sci.*, 2019, **20**, 4473.
40 X. Zhang, Y. Xiao, J. Qi, J. Qu, B. Kim, X. Yue and K. D. Belfield, *J. Org. Chem.*, 2013, **78**, 9153–9160.
41 S. S. Jalde, A. K. Chauhan, J. H. Lee, P. K. Chaturvedi, J.-S. Park and Y.-W. Kim, *Eur. J. Med. Chem.*, 2018, **147**, 66–76.
42 M. Asadi, S. Taghizadeh, E. Kaviani, O. Vakili, M. Taheri-Anganeh, M. Tahamtan and A. Savardashtaki, *Biotechnol. Appl. Biochem.*, 2022, **69**, 1633–1645.
43 P. Acedo, A. Fernandes and J. Zawacka-Pankau, *Fut. Sci. OA*, 2019, **5**, FSO366.
44 H.-W. Hsiao, C.-C. Yang and H. Masai, *Genome Instab. Dis.*, 2021, **2**, 263–280.
45 S.-K. Chiang, S.-E. Chen and L.-C. Chang, *Cells*, 2021, **10**, 2401.
46 V. Pittalà, L. Salerno, G. Romeo, M. N. Modica and M. A. Siracusa, *Curr. Med. Chem.*, 2013, **20**, 3711–3732.
47 M. Koizumi, T. Watanabe, J. Masumoto, K. Sunago, Y. Imamura, K. Kanemitsu, T. Kumagi and Y. Hiasa, *Sci. Rep.*, 2021, **11**, 22351.
48 M. Brown, W. Zhang, D. Yan, R. Kenath, L. Le, H. Wang, D. Delitto, D. Ostrov, K. Robertson, C. Liu and K. Pham, *PLoS One*, 2020, **15**, e0226917.
49 A. Chakraborty, R. Bose and K. Bose, *Front. Mol. Biosci.*, 2022, **9**, 824846.
50 S. Li, J. Sun, J. Yang, L. Zhang, L. Wang, X. Wang and Z. Guo, *Mol. Clin. Oncol*, 2013, **1**, 305–308.